












# Atmospheric Escape From Three Terrestrial Planets in the L 98-59 System

Emeline F. Fromont<sup>1,2</sup> , John P. Ahlers<sup>2,3</sup> , Laura N. R. do Amaral<sup>4,5,8</sup> , Rory Barnes<sup>6</sup> , Emily A. Gilbert<sup>7</sup> ,  
Elisa V. Quintana<sup>2</sup> , Sarah Peacock<sup>2,3</sup> , Thomas Barclay<sup>2,3</sup> , and Allison Youngblood<sup>2</sup> 

<sup>1</sup>Department of Astronomy, University of Maryland, College Park, MD 20742, USA

<sup>2</sup>NASA Goddard Space Flight Center, Greenbelt, MD 20771, USA

<sup>3</sup>University of Maryland, Baltimore County, Baltimore, MD 21250, USA

<sup>4</sup>Instituto de Ciencias Nucleares, Universidad Nacional Autónoma de México, Cto. Exterior S/N, C.U., Coyoacán, 04510 Ciudad de Mexico, CDMX, Mexico

<sup>5</sup>NASA NExSS Virtual Planetary Laboratory, Seattle, WA, USA

<sup>6</sup>Department of Astronomy, University of Washington, Seattle, WA 98105, USA

<sup>7</sup>Jet Propulsion Laboratory, California Institute of Technology, 4800 Oak Grove Drive, Pasadena, CA 91109, USA

Received 2023 June 14; revised 2023 November 12; accepted 2023 November 16; published 2024 January 18

## Abstract

A critically important process affecting the climate evolution and potential habitability of an exoplanet is atmospheric escape, in which high-energy radiation from a star drives the escape of hydrogen atoms and other light elements from a planet's atmosphere. L 98-59 is a benchmark system for studying such atmospheric processes, with three transiting terrestrial-sized planets receiving Venus-like instillations ( $4\text{--}25 S_{\oplus}$ ) from their M3 host star. We use the `vPlanet` model to simulate the evolution of the L 98-59 system and the atmospheric escape of its inner three small planets, given different assumed initial water quantities. We find that, regardless of their initial water content, all three planets accumulate significant quantities of oxygen due to efficient water photolysis and hydrogen loss. All three planets also receive enough strong X-ray and extreme-ultraviolet flux to drive rapid water loss, which considerably affects their developing climates and atmospheres. Even in scenarios of low initial water content, our results suggest that the JWST will be sensitive to observations of retained oxygen on the L 98-59 planets in its future scheduled observations, with planets b and c being the most likely targets to possess an extended atmosphere. Our results constrain the atmospheric evolution of these small rocky planets, and they provide context for current and future observations of the L 98-59 system to generalize our understanding of multiterrestrial planet systems.

*Unified Astronomy Thesaurus concepts:* [Exoplanet evolution \(491\)](#); [Exoplanet atmospheres \(487\)](#); [Star-planet interactions \(2177\)](#)

## 1. Introduction

To date, both ground-based radial velocity (RV) surveys and space-based transit surveys have found small ( $R < 1.6 R_{\oplus}$ ; Cloutier & Menou 2020) planets at higher occurrence rates around M dwarfs than for hotter stars (Bonfils et al. 2013; Dressing & Charbonneau 2013, 2015; Hardegree-Ullman et al. 2019; Ment & Charbonneau 2023). As of 2023 June, NASA's Exoplanet Archive lists 181 confirmed and 116 candidate small planets around M-dwarf stars. Additionally, many of these planets orbit nearby, bright stars, making them ideal candidates for atmospheric characterization by JWST (Gardner et al. 2006).

While hundreds of multiplanet systems have been discovered, only a limited number are amenable to follow-up observations. Most multiplanet systems have host stars that are too faint or have predicted signal amplitudes that are too small to be useful for follow-up mass and atmospheric measurements.

Situated at the border of JWST's continuous viewing zone (Demangeon et al. 2021), the L 98-59 system is an excellent benchmark target for JWST observations. As shown in Figure 1, the L 98-59 planets occupy an enticing region of

parameter space for follow-up study. The system is composed of four confirmed planets, L 98-59 b, L 98-59 c, L 98-59 d, and L 98-59 e, which orbit around their bright ( $K = 7.1$  mag) and nearby (10.6 pc; Kostov et al. 2019) M3 dwarf host star. The inner three small exoplanets, L 98-59 b, L 98-59 c, and L 98-59 d, reside interior to the system's habitable zone (HZ). Our work focuses only on these three planets, as L 98-59 e likely does not transit (Demangeon et al. 2021).

There is considerable value in modeling the evolution of the L 98-59 system, particularly because of a unique combination of characteristics including the presence of multiple terrestrial planets, their likely exposure to flares, and the system's overall ease of observation. These characteristics will allow us to better understand the interactions of planets around M dwarfs, climate development on Earth analogs, and potential habitability conditions that arise from such an environment.

The L 98-59 system presents an excellent opportunity to study the evolution and atmospheric characterization of multiple, small planets that formed in the same stellar environment (Greene et al. 2016; Morley et al. 2017; Demangeon et al. 2021). L 98-59 is the brightest and nearest M-dwarf star system that has at least two measured planetary masses and radii, as seen in Figure 2. While L 98-59 appeared to be a quiet star when it was first observed by the Transiting Exoplanet Survey Satellite (TESS; Ricker et al. 2015; Kostov et al. 2019), subsequent observations revealed stellar activity in the form of white-light flares. M-dwarf stars produce frequent flares across the electromagnetic spectrum (e.g., Muirhead et al. 2018; do Amaral et al. 2022) and remain active for long portions of their lifetimes (West et al. 2008, 2015). This

<sup>8</sup> Currently at *School of Earth and Space Exploration, Arizona State University, Tempe, AZ 85287, USA. Consortium on Habitability and Atmospheres of M-dwarf Planets (CHAMPs)*



Original content from this work may be used under the terms of the [Creative Commons Attribution 4.0 licence](#). Any further distribution of this work must maintain attribution to the author(s) and the title of the work, journal citation and DOI.

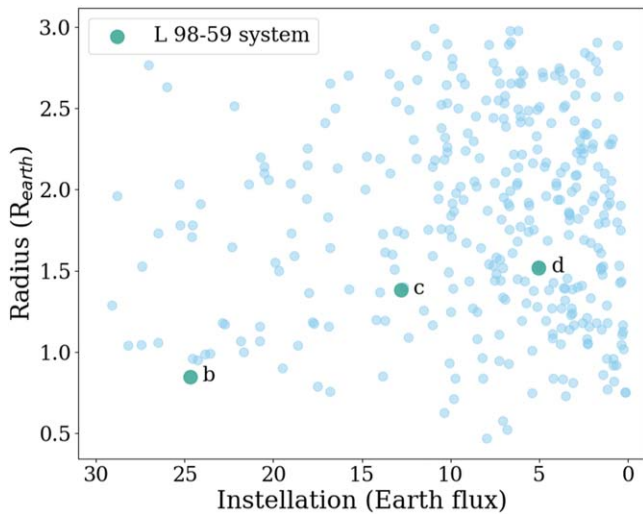


**Figure 1.** The radii and instellations of confirmed, transiting, multiplanet systems with planet radii  $< 3 R_{\oplus}$  and instellation  $< 30$  Earth fluxes. The L 98-59 planets are labeled in dark green with their corresponding names. Many of these planets are found at lower ( $< 12$  Earth flux) instellations, but the L 98-59 planets are spread out over a significant instellation range. The variation in radius and instellation within their same system presents an opportunity to study the evolution of different planets in the same stellar environment.

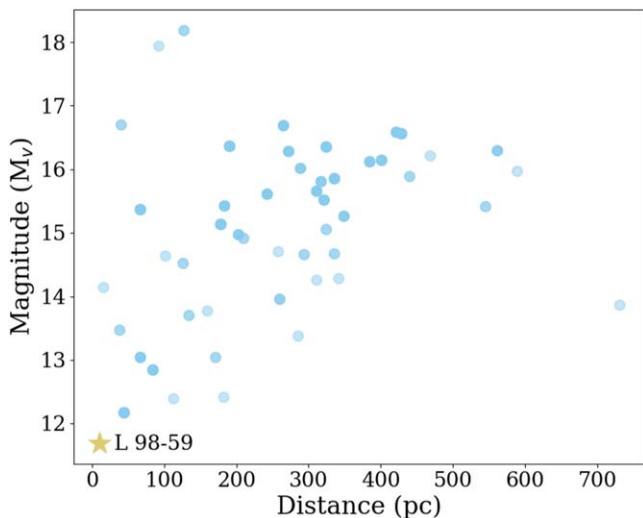


**Figure 2.** The distance from the Sun and V-band magnitude of the stars of the planetary systems plotted in Figure 1. Most of these systems are very faint and/or very distant, making them difficult to observe as atmospheric characterization targets. L 98-59 is both nearby and bright, making it a prime target for JWST observations.

activity likely affects planet atmospheres and must be accounted for in our atmospheric evolution models. Studying the atmospheres of planets orbiting active stars such as L 98-59 will provide us with a greater understanding of the effects of high-energy, or short-wavelength, radiation on the atmospheric retention and evolution of terrestrial planets over time.

Atmospheric escape is an important process to consider as part of the evolution and potential habitability of exoplanets. Strong X-ray and extreme-ultraviolet (XUV; 1–1000 Å; Ribas et al. 2005) radiation from the host star drives heating and ionization of the upper atmospheres of highly irradiated planets, leading to the escape of gases (Luger et al. 2015; Koskinen et al. 2022). XUV-driven escape is believed to have strongly affected the atmospheric evolution of solar system planets, such as Venus,

Earth, and Mars (Lammer et al. 2008), and is considered to be a likely culprit for sculpting the observed exoplanet population (Owen et al. 2020). Indeed, planets orbiting close to their host stars, like the L 98-59 planets, are particularly vulnerable to atmospheric escape. Transit observations by the Hubble Space Telescope (HST) in the far-ultraviolet (FUV) spectrum confirm that many planets close to their host stars lose mass to hydrodynamic escape, e.g., HD 209458b (Vidal-Madjar et al. 2003), HD 189733b (Lecavelier des Etangs et al. 2012), GJ 436b (Ehrenreich et al. 2015), and GJ 3470b (Bourrier et al. 2018). This can have important consequences not only for planets’ atmospheric evolution but for their structure and composition as well (Luger et al. 2015).

If the inner three planets of the system contained any volatiles in their initial composition, they should experience atmospheric escape because of their proximity to their star. To study the impact of XUV-driven escape on the L 98-59 planets, we use the modeling tool *vPlanet* (Virtual Planet Simulator; Barnes et al. 2020) to evolve the system over billions of years. By studying the atmospheric loss of this system, we hope to better understand the effects of an M dwarf’s stellar environment on the development of terrestrial-sized planets, which may impact their promise as potential targets for biosignature detection.

In the following sections, we describe our findings on the atmospheric evolution of the three inner planets in the L 98-59 system. We start by discussing the observational data and system properties of the L 98-59 system in Section 2. We then describe our planetary simulation model in Section 3. We interpret our model’s results in Section 4 and discuss their implications for future studies of the system in Section 5. Finally, we conclude with an overview of our results and their importance in the context of a new era of JWST observations in Section 6.

## 2. System Observations and Properties

### 2.1. Observations

TESS observed L 98-59 (TIC 307210830, TOI 175) for 21 sectors, up to and including Sector 69 (Burke et al. 2020). Kostov et al. (2019) initially reported the system’s discovery, in which they confirmed the presence of the inner three terrestrial planets (b, c, and d). Since then, Cloutier et al. (2019) and Demangeon et al. (2021) have provided planetary masses and eccentricities (Section 2.3). Although Demangeon et al. (2021) have recently confirmed the fourth planet, L 98-59 e (likely a rocky planet or a water world), we do not consider this planet in our model and analysis because it does not transit. We set our stellar and planetary parameters using the values displayed in Table 1.

Partly owing to L 98-59’s relative brightness for a host of small planets, it is an excellent transmission spectroscopy target with HST and JWST (see Section 5.2 for more detail). No atmospheric signal was conclusively detected by HST/Wide Field Camera 3 (WFC3) in five transits of planet b and one transit each for planets c and d. The data from planet b did not demonstrate any evidence for an atmosphere (Damiano et al. 2022), and the data collected for planet c were inconclusive, showing modulation in the transmission spectra that could be interpreted as evidence of an atmosphere, but at low significance (Barclay et al. 2023). Moreover, there were indications that the signal observed could be a result of contaminating signal from inhomogeneities in the stellar photosphere (Barclay et al. 2021, 2023). Two upcoming HST/WFC3 transits of planet c

**Table 1**  
Stellar and Planetary System Parameters

Parameter	Value Adopted for This Paper	Source
<b>L 98-59</b>		
Mass ( $M_{\odot}$ )	$0.273 \pm 0.030$	Demangeon et al. (2021)
Radius ( $R_{\odot}$ )	$0.303 \pm 0.0245$	Demangeon et al. (2021)
Temperature (K)	$3415 \pm 135$	Demangeon et al. (2021)
XUV saturation fraction	$0.002 \pm 0.001$	Peacock et al. (2020)
XUV beta exponent	$0.882 \pm 0.139$	Peacock et al. (2020)
XUV saturation time (Myr)	650	Peacock et al. (2020)
Age (Gyr)	>1	Demangeon et al. (2021)
Min. flare energy (erg)	$1.73 \pm 0.39 \times 10^{31}$	Barclay et al. (2023)
Max. flare energy (erg)	$7.14 \pm 0.88 \times 10^{31}$	Barclay et al. (2023)
<b>L 98-59 b</b>		
Mass ( $M_{\oplus}$ )	$0.4 \pm 0.155$	Demangeon et al. (2021)
Radius ( $R_{\oplus}$ )	$0.850 \pm 0.054$	Demangeon et al. (2021)
Density ( $\text{g cm}^{-3}$ )	3.6	Demangeon et al. (2021)
Flux ( $S_{\oplus}$ )	24.7	Demangeon et al. (2021)
Period (days)	2.2531136	Demangeon et al. (2021)
Semimajor axis (AU)	0.0218	Demangeon et al. (2021)
Eccentricity	0.103	Demangeon et al. (2021)
Inclination	0.0	Demangeon et al. (2021)
Argument of periastron (deg)	192	Demangeon et al. (2021)
Transit time (BJD <sub>TDB</sub> - 2457000)	1366.17067	Demangeon et al. (2021)
<b>L 98-59 c</b>		
Mass ( $M_{\oplus}$ )	$2.22 \pm 0.255$	Demangeon et al. (2021)
Radius ( $R_{\oplus}$ )	$1.385 \pm 0.085$	Demangeon et al. (2021)
Density ( $\text{g cm}^{-3}$ )	4.57	Demangeon et al. (2021)
Flux ( $S_{\oplus}$ )	12.8	Demangeon et al. (2021)
Period (days)	3.6906777	Demangeon et al. (2021)
Semimajor axis (AU)	0.0303	Demangeon et al. (2021)
Eccentricity	0.103	Demangeon et al. (2021)
Inclination	0.0	Demangeon et al. (2021)
Argument of periastron (deg)	261	Demangeon et al. (2021)
Transit time (BJD <sub>TDB</sub> - 2457000)	1367.27375	Demangeon et al. (2021)
<b>L 98-59 d</b>		
Mass ( $M_{\oplus}$ )	$1.94 \pm 0.28$	Demangeon et al. (2021)
Radius ( $R_{\oplus}$ )	$1.521 \pm 0.1085$	Demangeon et al. (2021)
Density ( $\text{g cm}^{-3}$ )	2.95	Demangeon et al. (2021)
Flux( $S_{\oplus}$ )	5.01	Demangeon et al. (2021)
Period (days)	7.4507245	Demangeon et al. (2021)
Semimajor axis (AU)	0.0484	Demangeon et al. (2021)
Eccentricity	0.0740	Demangeon et al. (2021)
Inclination	0.0	Demangeon et al. (2021)
Argument of periastron (deg)	180	Demangeon et al. (2021)
Transit time (BJD <sub>TDB</sub> - 2457000)	1362.73974	Demangeon et al. (2021)
<b>All planets</b>		
XUV absorption efficiency	0.15–0.3	Luger & Barnes (2015)
XUV absorption radius/planet radius	1.0	Luger & Barnes (2015)

may resolve the ambiguity in the results for L 98-59 c. Through Guaranteed Time Observations, JWST will observe L 98-59 c with NIRISS and L 98-59 d with NIRSpec.

## 2.2. Host-star Properties

L 98-59 is a small, main-sequence (MS) M3 dwarf star with a luminosity about 100 times fainter than our Sun ( $0.012 L_{\odot}$ ; Cloutier et al. 2019; Kostov et al. 2019; Demangeon et al. 2021). Due to its slow rotation, Kostov et al. (2019) estimated L 98-59's age to be >1 Gyr. Follow-up calculations by Demangeon et al. (2021) agree with this result, stating the

age of L 98-59 to be over 800 Myr. This star was also thought to be relatively quiet with little stellar activity, based on the lack of  $H\alpha$  emission in optical spectra (Kostov et al. 2019; Pidhorodetska et al. 2021). However, recent studies have confirmed the detection of flares on L 98-59 (Howard 2022; Stelzer et al. 2022; Barclay et al. 2023).

## 2.3. Planetary System Properties

There are four planets in the L 98-59 system, two of which are inferred to be rocky from their bulk densities. Initially, Cloutier et al. (2019) were unable to constrain the mass of

**Table 2**  
Optimistic and Conservative Habitable Zones of L 98-59

HZ Limit	Flux	Distance
Conservative		
Inner HZ	$0.9298 S_{\oplus}$	0.109 au
Outer HZ	$0.244 S_{\oplus}$	0.212 au
Optimistic		
Inner HZ	$1.492 S_{\oplus}$	0.086 au
Outer HZ	$0.22 S_{\oplus}$	0.224 au

L 98-59 b, instead defining an upper limit of 1.01 Earth masses ( $M_{\oplus}$ ). Demangeon et al. (2021) were later able to refine the planets’ masses to be  $0.4^{+0.16}_{-0.15}$ ,  $2.22^{+0.26}_{-0.25}$ , and  $1.94 \pm 0.28 M_{\oplus}$  for planets b, c, and d, respectively. As part of their RV analysis, Cloutier et al. (2019) also derived densities for L 98-59 c and d, determining planet c to have a rock-dominated composition and planet d to likely have a significant amount of water or gaseous atmosphere due to its lower density. Following up on their results, Demangeon et al. (2021) determined that the three inner planets have small iron cores, with densities  $3.6^{+1.4}_{-1.5} \text{ g cm}^{-3}$  (b),  $4.57^{+0.77}_{-0.85} \text{ g cm}^{-3}$  (c), and  $2.95^{+0.79}_{-0.51} \text{ g cm}^{-3}$  (d). Their analysis showed that planets b and c have very similar compositions, likely rocky and with a small mass fraction of water and a low gas mass, if any. On the other hand, their model favored a richer gas and water content for planet d.

Quick et al. (2020) reached similar conclusions in their volcanic and cryovolcanic analysis. Using estimates of the planets’ total internal heat, which includes both tidal heating and radiogenic heating, they estimated that L 98-59 b and c are likely to exhibit extreme volcanic activity at their surfaces. They also suggested that L 98-59 d may be an ocean world with some volcanic activity, based on the planet’s density and effective temperature.

The L 98-59 system resembles other multiplanet systems around M dwarfs, such as TRAPPIST-1 and Kepler-186 (Quintana et al. 2014; Gillon et al. 2017), in that M dwarfs frequently host compact, multiplanet systems (Muirhead et al. 2015; Kostov et al. 2019). At 0.0218 au (b), 0.0303 au (c), and 0.0484 au (d), the three inner planets reside interior to both the system’s conservative and optimistic HZ, as calculated from Kopparapu et al. (2013, 2014) using the values from Table 1. These HZ limit values are listed in Table 2. The system also follows the “peas in a pod” configuration initially described by Weiss et al. (2018), where within a multiplanet system planets tend to have similar sizes, and in systems with more than three planetary bodies planets tend to be evenly spaced in their orbits.

### 3. Numerical Methods and Models

#### 3.1. System Evolution Model

To study the atmospheric development of the L 98-59 planets, we simulate the evolution of the system over several billion years assuming an initial water content between 1 and 100 terrestrial oceans (TO) and accounting for the host star’s radiation and flares. We use the modeling software package VPLanet (Barnes et al. 2020) to model the atmospheric escape of the three innermost, terrestrial planets of the L 98-59 system. VPLanet is an open-source software for simulating the evolution of a planetary system, focusing specifically on habitability. By coupling various models, it allows users to incorporate specific modules and features into their planetary

system, such as tidal evolution or a circumbinary system. We will discuss each module we use in our model in Sections 3.1.1 (STELLAR), 3.1.2 (FLARE), and 3.1.3 (AtmEsc). We evolve the system from before the star’s MS phase (5 Myr) until the upper limit for the star’s age at the present day (13 Gyrs), in order to visualize the full timescale of this system’s evolution, which has previously been shown to be dynamically stable (Kostov et al. 2019; Demangeon et al. 2021).

We make three important assumptions in the initial setup of our model. First, we assume that the planets are in their currently observed orbits at the start of each simulation. We thus begin the simulations with the planets in their present orbits around L 98-59, and assume that any planet migration in the early stages of the system’s evolution has already taken place. This first assumption ties into our second one, in which we begin the simulations before the star’s MS phase, at a stellar age of 5 Myr. Pre-main-sequence (PMS) M dwarfs emit higher amounts of flux in the XUV as compared to MS stars (Ramirez & Kaltenegger 2014; Luger & Barnes 2015; Tian & Ida 2015; do Amaral et al. 2022). Excess XUV flux can cause more water loss and oxygen accumulation early in a planet’s evolution, so it is important to include that early evolution time in our simulations; by not doing so, we might severely underestimate the desiccation of the L 98-59 planets. Third, we assume that all three planets start with the same water mass at the beginning of each simulation. This allows us to directly compare the effects of L 98-59’s stellar activity and evolution on each planet in the system, and, in turn, how water content changes on each of them.

We investigate the evolution and outcome of three different atmospheric-escape scenarios by varying the initial water content of the L 98-59 planets. Do Amaral et al. (2022) found that the amount of escaping water is independent from the starting quantity of water on a planet, and that the star mass is inversely correlated with the amount of water lost. In other words, planets tend to lose the same amount of water regardless of their initial budget, and smaller stars will contribute most to this water loss due to their longer PMS phase. Given we do not know the underlying initial water budget for the L 98-59 planets, we vary the starting water budgets in order to gain a broader understanding of the water retention on each planet over time.

We vary the water budgets, running sets of simulations with initial water masses of 1, 10, and 100 TO following the procedures of Morbidelli et al. (2000), Raymond et al. (2006), Chassefière et al. (2012), Luger & Barnes (2015), and do Amaral et al. (2022) in order to account for the possibility of the planets forming in situ, or migrating in from further out in the disk where more water may have been available at planet formation (Mordasini et al. 2012; Tian & Ida 2015; Unterborn et al. 2018; Pidhorodetska et al. 2021). Our parameter variation method is further discussed in Section 3.1.4.

We describe the specific modules used in our model in the following subsections. Using the VPLanet modules STELLAR and FLARE, we account for both XUV and flare activity from the L 98-59 star in our model. We also use the AtmEsc module to simulate the planets’ atmospheric and oceanic evolution over time.

##### 3.1.1. STELLAR Module

As a star evolves and ages, the changes in its stellar activity affect the formation, evolution, and potential habitability of its surrounding planets. Early M stars, such as L 98-59, emit near-constant elevated levels of XUV flux for the first few hundred

million years before decreasing with time ( $\sim t^{-1}$ ) by 2 orders of magnitude toward field age (Peacock et al. 2020). This decrease in emission is linked to the spin down of the star reducing the dynamo production of its magnetic field (West et al. 2015).

The STELLAR module allows users to include the star’s changing parameters in the system evolution model, including its XUV parameters and stellar evolution model (Baraffe et al. 2015). Following the results from Peacock et al. (2020), we adopt an XUV saturation timescale of 650 Myr for L 98-59. To determine the XUV saturation fraction and  $\beta$  exponent for L 98-59, we use evolutionary models of  $0.35 M_{\odot}$  stars from Peacock et al. (2020)<sup>9</sup> in combination with the ROSAT X-ray measurements of proxy stars from Shkolnik & Barman (2014) to create full panchromatic spectra representative of L 98-59 at ages between 10 Myr and 5 Gyr.<sup>10</sup> We use the Peacock et al. (2020) models for wavelengths  $>100 \text{ \AA}$  and the ROSAT measurements for wavelengths  $<100 \text{ \AA}$ . We compute the XUV (1–1000  $\text{\AA}$ ) and bolometric luminosities from these spectra and fit a power law to the decreasing  $L_{\text{XUV}}/L_{\text{bol}}$  to determine the  $\beta$  exponent (the coefficient in this power-law fit). We do this with the median models for each age and the inner quartile models to provide an uncertainty:  $\beta = 0.882 \pm 0.139$ . The XUV saturation fraction is  $L_{\text{XUV}}/L_{\text{bol}}$  at the saturation time of 650 Myr,  $L_{\text{XUV}}/L_{\text{bol}} = 0.002 \pm 0.001$ .

### 3.1.2. FLARE Module

The presence of flares in a planetary system can have a strong impact on the habitability of a planet, particularly on the retention and detection of its atmosphere. Flares can alter the chemical composition of a planet’s atmosphere, and repeated exposure to flares can cause a planet to quickly lose any atmosphere it might have accumulated (Tilley et al. 2019; Chen et al. 2021; Louca et al. 2023). Until now, little work has been done to study the impacts of flare exposure on a planet’s ocean retention, even though the most commonly observed stars for small, rocky exoplanet characterization—MS M stars, or M dwarfs—are known to emit such radiation (Billings 2011; Shields et al. 2016; Fujii et al. 2018; do Amaral et al. 2022). Our evolution model thus includes the effects of flares on the atmospheric escape and ocean retention of the L 98-59 planets.

The FLARE module in VPLANET enables users to specify basic information on the star’s flare distribution. We identify eight flares in Sector 11 of TESS observations using a modified version of `bayesflare` (Pitkin et al. 2014) as described in Gilbert et al. (2022). Using the identified flare parameters (peak time, amplitude, and FWHM) as identified in the flare detection, we model these flares using `xoflares` (Barclay & Gilbert 2020). We integrate under these models to determine the equivalent duration of each flare, then scale these to absolute energies using the convolution of an M3 spectral model of L 98-59 and the TESS bandpass. From here, we determine the mean energy of the star and then use the model of the individual flares from Barclay et al. (2023) to determine the minimum and maximum flare energies, which are  $1.73^{+0.38}_{-0.41} \times 10^{31}$  erg and  $7.14^{+0.88}_{-0.88} \times 10^{31}$  erg, respectively. These uncertainties are

<sup>9</sup> <https://stdatu.stsci.edu/hlsp/hazmat>

<sup>10</sup> 5 Gyr is the oldest spectrum available from Peacock et al. (2020). At X-ray wavelengths (1–100  $\text{\AA}$ ), we adopt a single-value flux consistent with the median ROSAT measurement for each given age bin. Since the XUV flux declines in a consistent manner beyond 650 Myr, calculating the XUV saturation fraction and  $\beta$  exponent with models between 650 Myr and 5 Gyr (rather than 13 Gyr) yields a sufficiently long baseline to use.

averaged such that we use a minimum flare energy of  $1.73 \pm 0.39 \times 10^{31}$  erg and a maximum flare energy of  $7.14 \pm 0.88 \times 10^{31}$  erg. We use the “TESSUV” option for the “sFlareBandPass” parameter, which follows Günther et al. (2020) to calculate which fraction of the bolometric energy for observed flares falls into the U band ( $E_U \approx 7.6\% E_{\text{bol}}$ ).

### 3.1.3. AtmEsc Module

Atmospheric escape is the process undergone by a planet when gases from its atmosphere are lost to space. There are two broad categories of atmospheric escape defined by the gas-loss mechanism: thermal escape and nonthermal escape. Thermal escape includes Jeans escape, in which the temperature of a gas accelerates its particles to above the escape velocity, and hydrodynamic escape, in which escaping gas molecules drag along other molecules, creating a fluid-like escape behavior. Nonthermal escape includes processes such as photochemical loss, ion loss, and ionospheric outflow (among others), and generally involves more complex interactions in ions and plasma (see Gronoff et al. 2020 for more detail on atmospheric-escape processes).

Thermal escape is considered the dominant mechanism for highly irradiated planetary atmospheres, so the VPLANET model includes energy-limited and diffusion-limited escape for H/He and water-vapor atmospheres. Energy-limited escape occurs as a hydrodynamic wind “blows away” hydrogen in the atmosphere, and is driven by a fixed fraction of the incoming XUV energy. However, if not all of the oxygen escapes and some remains in the atmosphere, the hydrogen will have to escape by diffusing through a background of oxygen in the atmosphere, thus causing diffusion-limited escape (Luger & Barnes 2015).

The AtmEsc module in VPLANET describes the evolution of a planet’s atmosphere and ocean retention. We specify each planet’s starting water budget as 1, 10, or 100 TO, and vary this quantity in a way that is further discussed in Section 3.1.4. We follow the water-loss model described in Luger & Barnes (2015) to simulate the evolution of water on each planet and to set some of our parameters. We set the XUV absorption radius to be equal to the planet radius, since XUV radiation is absorbed in the uppermost layers of a planet’s atmosphere, and we set the XUV absorption efficiency parameter to vary between 0.15 and 0.3. We select the model from Bolmont et al. (2017) in the VPLANET code to determine the XUV absorption efficiency parameter for water vapor. In these simulations, we assume minimal  $\text{O}_2$  absorption at the surface (Lincowski et al. 2018), so we do not include  $\text{O}_2$  loss processes other than the ones built into the VPLANET integrator. We also assume no significant H/He envelopes. We keep the Jeans time, in which the ballistic escape of individual atoms drives atmospheric mass loss in the low-temperature limit (Luger et al. 2015), to the default value of 1 Gyr.

### 3.1.4. Parameter Variation

In order to consider the full range of scenarios for the system’s evolution, we vary the following parameters within their uncertainties: star mass ( $M_s$ ), planet mass for all three planets ( $M_p$ ), planet radius for all three planets ( $R_p$ ), XUV saturation fraction, XUV beta exponent, minimum flare energy, and maximum flare energy. Using Monte Carlo sampling, we draw 1000 values from a Gaussian distribution for each of these parameters. We also include each planet’s XUV

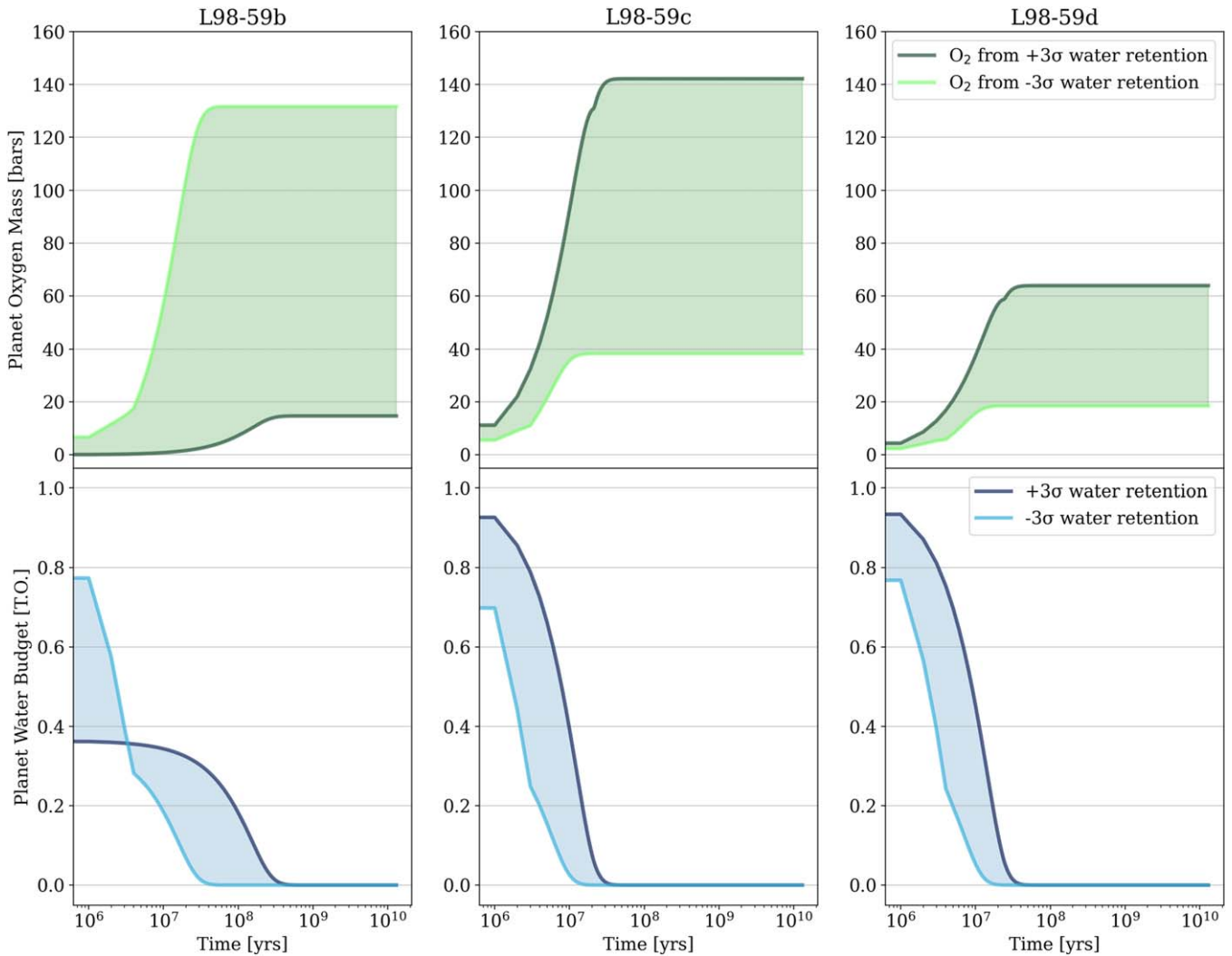


**Figure 3.** 1 TO: these plots show the range of outcomes for oxygen accumulation (top row, green) and water retention (bottom row, blue) for the set of simulations with 1 TO initial water content on planets b (left column), c (middle column), and d (right column). The dark and light blue lines represent the simulations corresponding to the  $+3\sigma$  and  $-3\sigma$  (respectively) of the water desiccation times distribution for each planet at 1 TO. These distributions can be found in Figure 6, top row. The dark and light green lines correspond to the same simulations as the ones chosen in the water behavior plots. Given 1 TO, water is not likely to survive past 1 Gyr for any planet, which makes water observations more unlikely. However, the quantities of oxygen produced are still significant—up to 140 bars. Notice that for planet b, simulations that retain water longer are the ones that accumulate the least oxygen, contrary to planets c and d. These b simulations also show a quick initial drop in water content, and then a slower loss over time than the simulations that retain water for shorter times. This is due to a high XUV flux for b, which increases radiative cooling and decreases escape efficiency. Further detail is provided in Section 4.

absorption efficiency in our sampling as a flat distribution from 0.15 to 0.3, which is considered the range appropriate for planets with hydrogen-rich atmospheres around M dwarfs (Luger & Barnes 2015). We then use these varying parameters to generate 1000 unique simulations, spanning the parameter space of the L 98-59 system. We will refer to these 1000 simulations as a *set* of simulations. We fix all other parameters in the model, excluding the semimajor axis, which varies indirectly due to Newton’s version of Kepler’s third law.

We perform a set of simulations for three initial water masses: 1, 10, and 100 TO on each planet. For each initial water budget, we simulate the instellation and each planet’s climatic response using input parameters as described above to build a distribution of water-loss and atmospheric-escape scenarios. In our model, we consider “desiccated” to mean that a planet’s water content has dropped to zero. We note that this may affect the interpretation of our results, as even simulations that retain insignificantly small amounts of water are still considered nondesiccated. Thus, we

model 1000 total scenarios per starting water budget, with which we determine the range of most likely scenarios within  $3\sigma$  for water retention and oxygen accumulation on the L 98-59 planets. That is, given the distribution of our simulation results, we find the water-evolution scenario at  $+3\sigma$  to represent the “most” or “longest” water retention and the water-evolution scenario at  $-3\sigma$  to represent the “least” or “shortest” water retention, giving us a range of most likely water and oxygen evolution behaviors for each planet.

#### 4. Results

The main results from our simulations, showing the water retention and oxygen accumulation over time for the L 98-59 planets at different starting water budgets, are summarized in Figures 3, 4, and 5. We find that all three planets are experiencing strong atmospheric escape due to their proximity and exposure to their star’s XUV and flare activity. All three

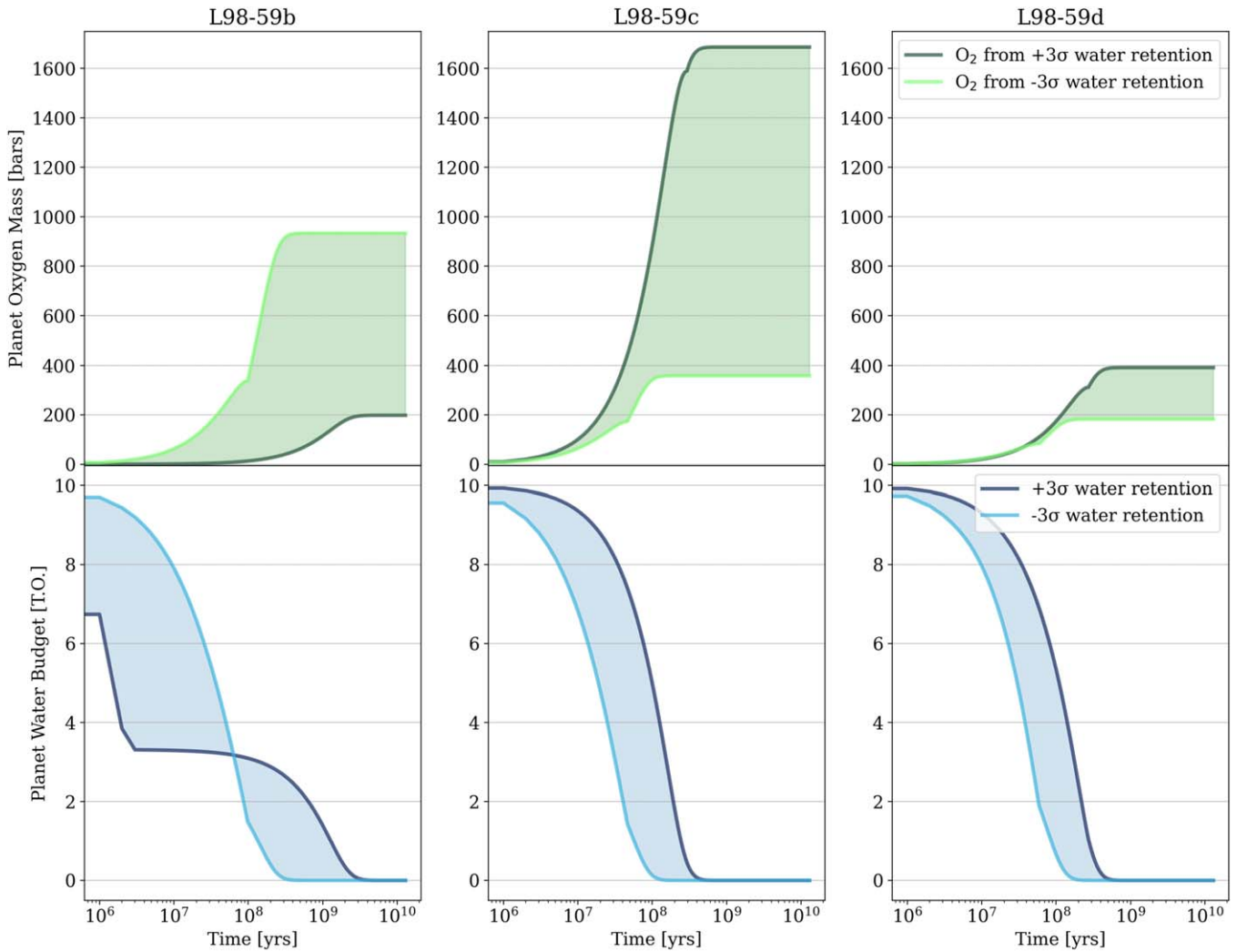


**Figure 4.** 10 TO: these plots show the range of outcomes for oxygen accumulation (top row, green) and water retention (bottom row, blue) for the set of simulations with 10 TO initial water content on each of the planets. The distributions for the water behavior can be found in Figure 6, middle row. Given 10 TO, all three planets can accumulate hundreds of bars of oxygen, and planet b is likely to retain water for longer than planets c and d (likely past 1 Gyr), making water detections more likely for this planet. However, depending on the system’s age, all three planets may still have some water left. Details on planet b’s behavior, similar to Figure 3, are given in Section 4.

planets are able to accumulate significant quantities of oxygen in their atmospheres over time. While all three planets display significant water loss, planet b shows the potential for water retention when given a medium to high initial water content, but planets c and d are unlikely to retain significant amounts of water unless given a high initial water content.

As seen in the histograms from Figure 6, when given 100 TO of starting water, most of the simulations predict that planet b will not desiccate and will instead retain some fraction of water, as opposed to planets c and d, which still tend to desiccate in this situation. At higher XUV fluxes, such as ones that planet b experiences, the escape efficiency decreases due to increased radiative cooling. This means that less hydrogen is escaping, but that which is escaping leaves the atmosphere at a high velocity and drags along large amounts of oxygen with it (Tian et al. 2008; Bolmont et al. 2017). Note that although planet b retains water in most cases given 100 TO, the surviving simulations still likely have very little water left over (see Figure 7).

Planets c and d are both less likely than planet b to retain significant amounts of water over long periods of time, unless they begin evolving with high quantities of water. Indeed, most

of our *VPlanet* simulations predict that in cases of 1 TO and 10 TO of initial water, planets c and d completely desiccate before 1 Gyr, as seen in Figures 3, 4, and 6, unless they start their evolution with a significant amount of water. Given 100 TO, planet c is able to retain water for close to 11 Gyr (Figure 6, bottom middle), and planet d shows a few cases of retaining water for more than 13 Gyr (Figure 6, bottom right).

The atmospheric escape resulting from the star’s intense XUV radiation causes the planets to accumulate significant quantities of oxygen, in both low and high initial water content cases. Given 1 TO, the planets can accumulate from around 15 bars up to more than 140 bars of  $O_2$ . In addition, given 100 TO the planets can accumulate thousands of bars of  $O_2$ . Unless the planets began their orbits completely desiccated and stripped of any volatiles, there is a strong chance of observing secondary atmospheres dominated by oxygen on all three of them. We note that these simulations do not take into account potential volcanic activity on the planets, which, as discussed in Section 2.3, is a likely scenario for planets b and c. This implies that the planets may also accumulate other volatiles produced by volcanic outgassing, besides  $O_2$ . Our simulations

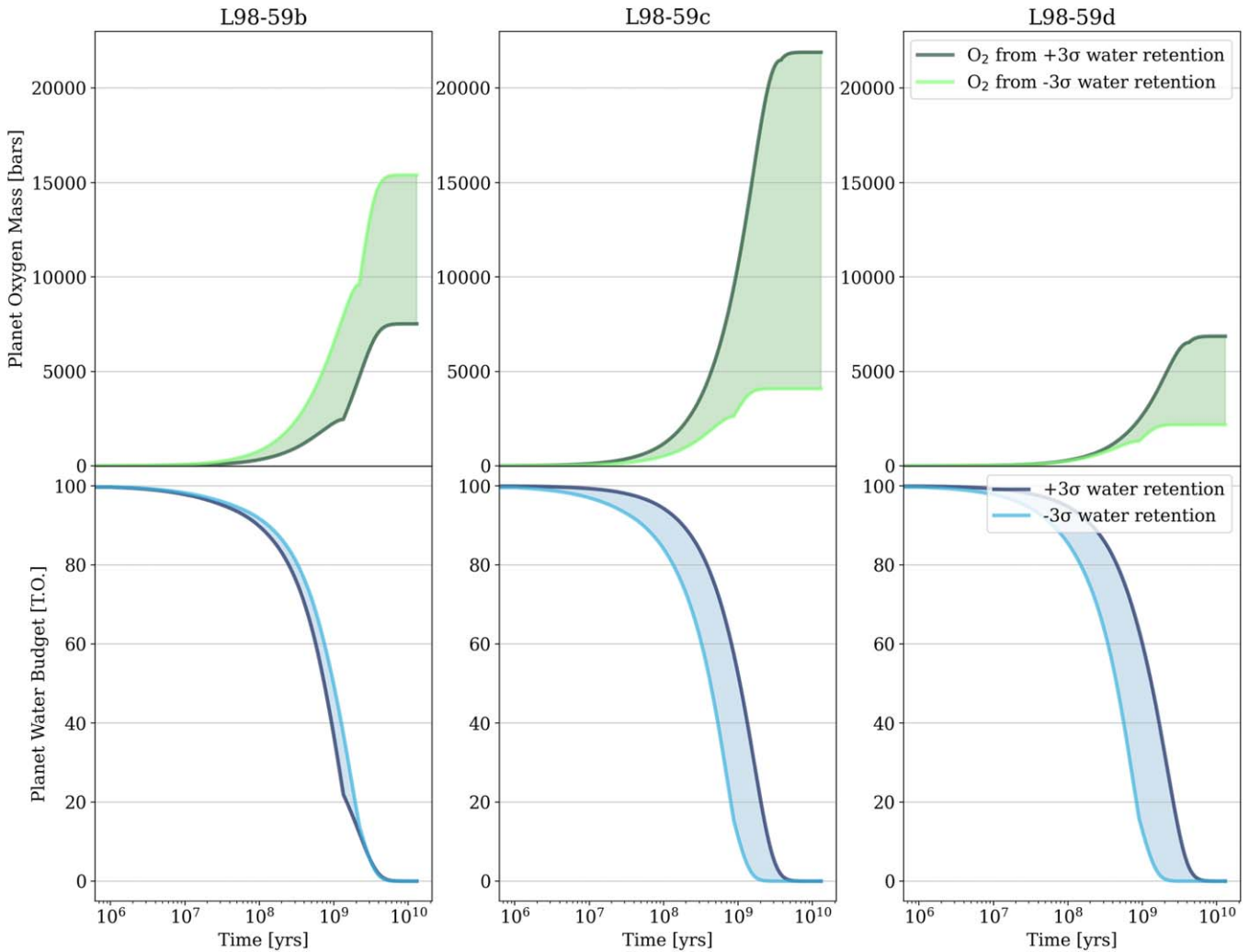


**Figure 5.** 100 TO: these plots show the range of outcomes for oxygen accumulation (top row, green) and water retention (bottom row, blue) for the set of simulations with 100 TO initial water content on each of the planets. The distributions for the water behavior can be found in Figure 6, bottom row. Given 100 TO, all three planets are likely to retain water past 1 Gyr, making observations of water relatively likely. In addition, thousands of bars of oxygen may be produced for each planet in this scenario. Details on planet b’s behavior, similar to Figure 3, are given in Section 4.

also do not account for potential sinks, like magma oceans; this is further discussed in Section 5.4.

Examining the water evolution displayed in Figures 3, 4, and 5, we find that the water loss and oxygen accumulation over time consistently do not behave the same way for planet b as they do for planets c and d. For planet b, the simulations that seem to retain water for shorter periods of time have a rather fast and steady water-loss rate right from the beginning, which only slows down when the planet reaches insignificant levels of water. However, the simulations that seem to retain water for longer begin their evolution with an instantaneous drop in water quantity, and then continue with a much slower water-loss rate. These simulations also accumulate much less oxygen than simulations with shorter water retention times. By contrast, planets c and d display a more constant water-loss rate in all simulations throughout the sets, and their simulations that retain water the longest also accumulate the most oxygen.

This opposing behavior in water loss and oxygen retention is related to how the escape efficiency depends on the XUV flux, for the same reason why planet b is more likely than the other planets to retain some water, given a high initial water content. Planet b experiences a higher XUV flux than the other planets,

such that it has a lower escape efficiency and could then retain water for longer. But with a high XUV flux, the hydrolyzed oxygen that does accumulate in the atmosphere will be dragged away by quickly escaping hydrogen. Planets c and d, with a higher escape efficiency, will experience a steeper and more constant water loss. Exposure to a less intense XUV flux also means that they can accumulate more oxygen, since it does not get carried away by hydrogen as dramatically as for planet b.

## 5. Discussion

### 5.1. L 98-59 Planets Are in a Runaway Greenhouse

The L 98-59 planets have mean semimajor axes values of 0.0218 au (b), 0.0303 au (c), and 0.0484 au (d), and thus have instellations ranging from about 4–25 times the instellation that the Earth receives from the Sun (Figure 1). These planets therefore fall firmly in the Venus zone (Kane et al. 2014; Ostberg et al. 2023), the region around a star within which a planet like Earth with water on its surface would likely have been forced into a runaway greenhouse. Most Venus analogs have been found around faint stars for which it is difficult to obtain follow-up measurements. However, the L 98-59 planets’

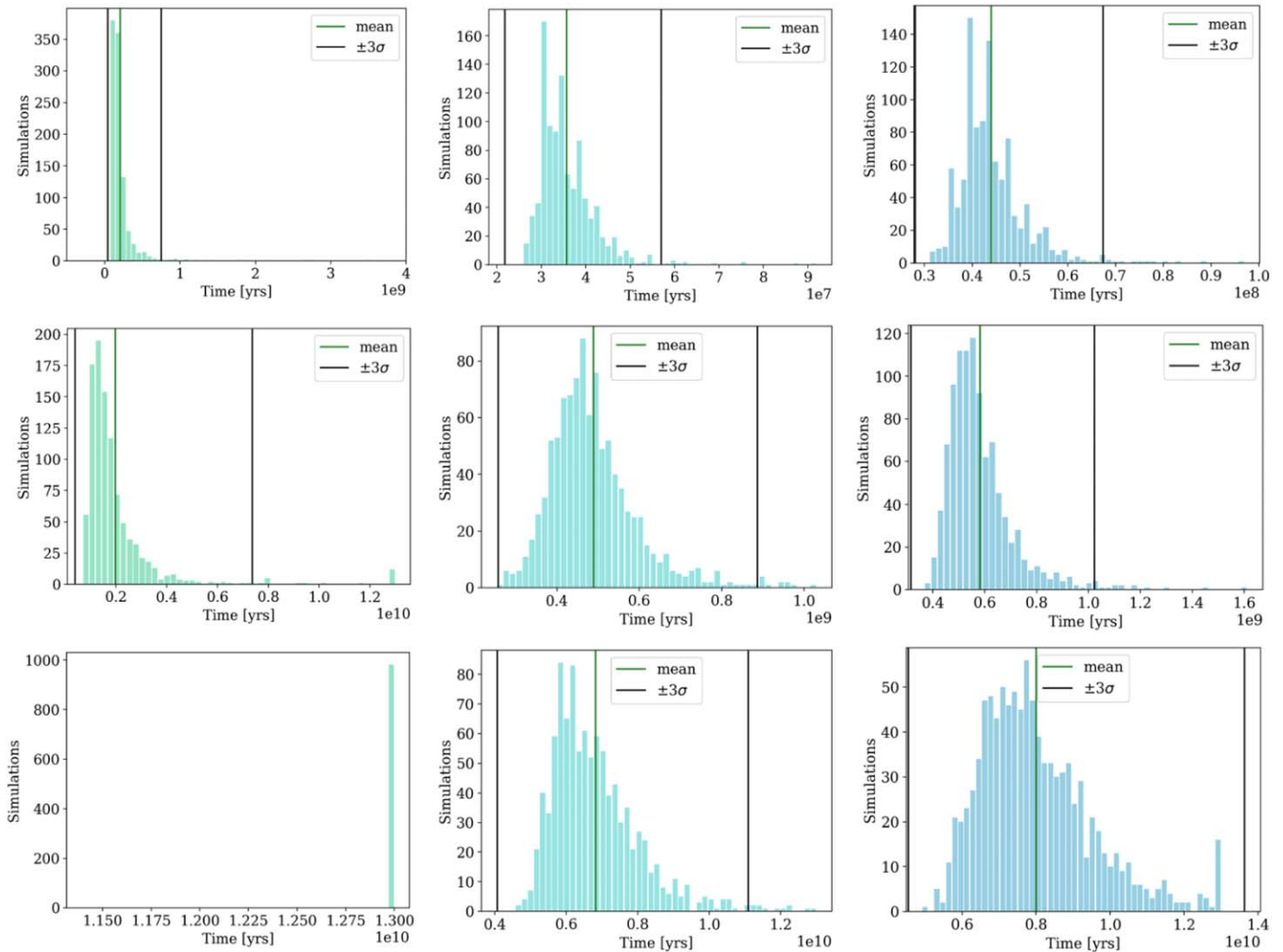


**Figure 6.** These plots show the distribution of the water desiccation times for the set of simulations run at 1 TO (top row), 10 TO (middle row), and 100 TO (bottom row) for planets b (left column, green), c (middle column, light blue), and d (right column, dark blue), spread out over 50 bins. The vertical green line and the vertical black lines in each plot show the log mean and  $\pm 3\sigma$  of the results distribution, respectively. In all three initial water cases, planet b on average retains water the longest. In the bottom-left histogram, the fullest bin on the far right of the plot shows all cases of water survival for planet b at 100 TO. Note that the cases of water survival only accumulate in the 1.3 Gyr bin, as the simulations all stopped at 1.3 Gyr. Although it seems like all the simulations retained water in planet b’s 100 TO case, a few simulations being obscured by the magnitude of the surviving cases were fully desiccated. A distribution of only the desiccated cases and a distribution of only the surviving-water cases for planet b can be found in Figure 7.

location along with the brightness of their host star create a convenient combination that would allow us to learn more about the evolution and atmospheric development of Venus-like planets (Pidhorodetska et al. 2021). L 98-59 c and d, if they have atmospheres, are prime JWST targets to observe and study potential Venus analogs and further study the origin and backstory of our sister planet (Kane et al. 2019).

As seen in Figures 3, 4, and 5, the L 98-59 planets are likely experiencing a runaway greenhouse, which makes them an excellent target for JWST observations of evolving atmospheres and unstable climates. In a runaway greenhouse state, the planets’ surface temperatures exceed the critical point of water (647 K) and their oceans start evaporating (Kasting 1988; Abe 1993; Kasting et al. 1993). Our simulation results show that all three planets are constantly losing water and accumulating high quantities of oxygen from water photolysis, because they are so small and so close to their star. Schindler & Kasting (2000) modeled synthetic spectra of hypothetical Earth-like atmospheres, which showed that “Venus-like”

planets could conceivably accumulate large amounts of oxygen in their atmospheres. Luger & Barnes (2015) confirmed this behavior in their planetary evolution and water-loss model, demonstrating that planets around the HZ of M-dwarf stars may develop atmospheres with hundreds to thousands of bars of  $O_2$ . Thus, if the three planets had started their evolution with any nonnegligible water budget, it is likely that they would display signs of water loss and volatile accumulation in their atmospheres. Any detection of volatiles on the L 98-59 planets would show an impermanent state in the lifetime of the system, but would also offer real-time snapshots of a runaway greenhouse state and its effects on the climate stability and evolving atmospheric composition of a planet.

## 5.2. Potential Future Volatile Detections

Depending on the system’s age, there is a real possibility of observing potential water signatures on L 98-59 b, as it seems prone to longer water retention than L 98-59 c and d. Additionally, our simulations predict a significant accumulation

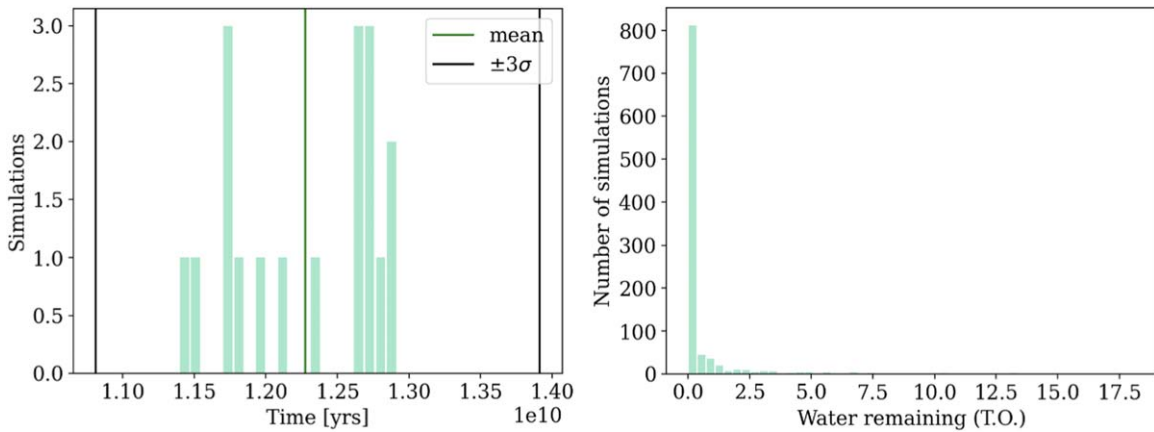


**Figure 7.** This plot shows the distribution of the desiccated cases (left) and the surviving-water cases (right) for the set of simulations run at 100 TO for planet b, as seen on the bottom-left plot of Figure 6. The desiccated cases plot shows when simulations ran out of water before 13 Gyr, spread over 20 bins, and the surviving-water cases shows how much water remained in simulations that survived past 13 Gyr. We use different bin numbers for both plots because very few cases fully ran out of water before the end of our simulation time. The vertical green line and the vertical black lines on the left plot show the log mean and  $\pm 3\sigma$  of the results distribution, respectively. Note that although planet b desiccated in very few simulations given 100 TO, most cases that made it past 13 Gyr still had very little water remaining. However, it is interesting to consider that, depending on the L 98-59 system’s age, planet b may still have some water present.

of oxygen in planet b’s atmosphere, especially in the case of 100 TO. Such quantities of oxygen and water vapor, resulting from water loss, may create a haze in the planet’s atmosphere, thus obscuring potential water signal detections. Indeed, a recent transmission spectrum of L 98-59 b, found to be relatively flat, predicts that planet b either has no atmosphere or an atmosphere with high-altitude clouds or haze (Damiano et al. 2022). The authors’ data rule out a cloud-free and H<sub>2</sub>-dominated atmosphere, which is consistent with our initial assumptions about the planet. However, this transmission spectrum does not favor a water-vapor-dominated atmosphere either, although the possibility remains if clouds are included in the model.

JWST observations of planet b in parallel with planets c and d would provide essential information on the evolution of different planets around the same M dwarf. Not only would it allow us to compare the development and loss of atmospheres on three small planets in the same system, but the detection of H<sub>2</sub>O on L 98-59 b would allow us to place constraints on evolutionary scenarios, by looking at how oceans and atmospheres behave when subjected to such intense irradiation. For example, we may determine whether these planets formed with a large initial amount of water, giving us a way to probe into the mechanism of volatile accumulation during the initial formation stage of planets.

Thanks to the sensitivity of its instruments, JWST would be capable of detecting the presence of oxygen on the L 98-59 planets. Planets b and d of the system are both listed in the best-in-class planet candidates list compiled by Hord et al. (2023) for having the potential to yield high-quality spectra. This list accounts for the sensitivity of JWST’s instruments and shows that these L 98-59 planets have a relatively high transmission spectroscopy metric (or TSM; Kempton et al. 2018). Additionally, Pidhorodetska et al. (2021) performed simulations using the Planetary Spectra Generator (Villanueva et al. 2018) to determine the detectability of different atmospheric features on the L 98-59 planets by JWST. Specifically, they predict that NIRISS SOSS, and even MIRI LRS, would be capable of detecting the apparent features of a desiccated O<sub>2</sub> atmosphere (see Figures 8 and 9 from Pidhorodetska et al. 2021 for further detail). Although ozone (O<sub>3</sub>) can result from the

photochemical processing of O<sub>2</sub>, the L 98-59 planets should have hot enough atmospheres that O<sub>3</sub> production would be significantly reduced, making it unlikely that these features would interfere with potential O<sub>2</sub> detections. However, we note that our results predicting high quantities of oxygen on the L 98-59 planets represent an *upper limit* on the accumulation of oxygen. Because the potential presence of oxygen sinks on the planets would decrease the available atmospheric oxygen, we should interpret these results as describing how much oxygen the XUV radiation of a star can produce on volatile-rich planets, rather than how much oxygen will be available to detect.

### 5.3. Assumptions Regarding Flares and Water Delivery

As an M dwarf, L 98-59 is more prone to stellar variability and flares, which presents a challenge for the planets’ ability to retain any significant atmosphere or ocean. XUV radiation emitted by M dwarfs heats the exosphere of a planet’s atmosphere, causing the exobase to expand, and therefore facilitating escape (Murray-Clay et al. 2009; France et al. 2020). Thus, continuous exposure to repeated flaring can significantly deplete an atmosphere (Tilley et al. 2019; France et al. 2020). It is likely that any water on the L 98-59 planets would be significantly affected, if not desiccated, by the star’s flares and intense XUV radiation, as water-rich atmospheres may be severely depleted during a star’s PMS phase (Luger & Barnes 2015; Tian & Ida 2015; do Amaral et al. 2022).

In addition, flares can generate up to hundreds of bars of additional O<sub>2</sub> due to water photolysis (do Amaral et al. 2022), and planets in an extended runaway greenhouse in the HZ of M dwarfs can also accumulate hundreds to thousands of bars of O<sub>2</sub> (Luger & Barnes 2015). So while these atmospheric-escape processes might create detectable amounts of oxygen on the L 98-59 planets, we note that this would be a false biosignature and an unreliable measure of the habitability of these planets (Domagal-Goldman et al. 2014; Tian et al. 2014; Wordsworth & Pierrehumbert 2014; Luger & Barnes 2015). Although M dwarfs like L 98-59 may seem unfavorable hosts to habitable planets, with the combination of many evolutionary factors there is still a chance for them to host volatile-rich worlds, and

they remain important targets to study terrestrial planets subject to frequent high levels of XUV radiation.

The presence of water on the L 98-59 planets is highly dependent on their composition, which is in turn dependent on their formation process and location. There are three possible formation scenarios: (i) formation at their present location, (ii) formation further out in the disk and inward migration to their current locations, and (iii) gravitational scattering causing the planets to shift their orbits to their current locations (Ogihara & Ida 2009; Chiang & Laughlin 2013; Ciesla et al. 2015). The L 98-59 planets orbit extremely close to their star, so it is most likely that they have migrated inward during the early stages of the system’s formation (Ogihara & Ida 2009; Pu & Lai 2019). Simulations by Raymond et al. (2007) also show that it is difficult to form planets larger than  $0.3 M_{\oplus}$  so close to a low-mass star. Given the predictions of studies by Ogihara & Ida (2009) and Ciesla et al. (2015), we consider there to be a significant likelihood for the L 98-59 planets to be composed of a nonnegligible proportion of volatiles, including water, by the time they have fully formed and reached their current orbits.

#### 5.4. Limitations of This Work

While our simulations show a range of outcomes that fall relatively in line with predictions from previous works, we note that they may not fully capture the specific details of the L 98-59 system’s evolution. As established by Barnes et al. (2020), the `AtmEsc` module of the `VPLanet` model is only an approximate description of atmospheric escape, and does not include some processes present in small, terrestrial planets, including the wavelength dependence of upper-atmosphere heating and its variation with composition and atmospheric temperature structure, line-cooling mechanisms, and other nonthermal escape processes. It also does not include  $\text{CO}_2$ , which is a very common volatile and likely to be found in the atmospheres of planets. But while the `VPLanet` model does not account for some known effects in the evolution of terrestrial planets, we believe that the results obtained give us a good estimate of the general state of the L 98-59 planets. More importantly, it provides us with a strong baseline for comparison with future observations of this system, or others like it. This general knowledge can (i) be a benchmark for what to expect when observing similar systems, (ii) help us to interpret these future observations, and (iii) refine our models and understandings of the evolution of small, multiplanet systems around M dwarfs.

Our simulations assume that no magma ocean is present on the planets. However, like many planetary-sized bodies, the L 98-59 planets were likely molten right after their formation, a state known as a magma ocean (Solomon 1979; Wetherill 1990; Lammer et al. 2018). This would affect their initial volatile budget, how much oxygen may accumulate, and how fast water is lost. During a magma-ocean state, oxygen not only accumulates in the atmosphere but may also enter the melted surface, the latter which could outgas  $\text{H}_2\text{O}$  as a result (see Barth et al. 2021). These potential composition differences would affect the quantity of oxygen and water in the atmosphere, the quantity of oxygen stored in the planet, and the quantity of water produced by the magma ocean. Perhaps this would decrease the amount of oxygen in the atmosphere, and allow any water present to be “protected” by the magma ocean and retained longer. We note that future works could include this magma-ocean state for a more complete picture of the L 98-59 planets’ evolution.

The age of L 98-59 is poorly constrained, and yet stellar age strongly affects what state the system’s planets find themselves in. While the actual age of the star does not affect our results, since our simulations run from the star’s PMS until the maximum age that the star could be, the age *does* affect the implications of our results and the coupled interpretation of observations of these planets. Future JWST observations of the system would inform us of the age of the system and the starting water budget of the planets. Similarly, further constraints on the age of L 98-59 would affect our interpretation of our model results, thus further constraining the atmospheric state of the planets. For example, recent work by Engle & Guinan (2023) finds an updated stellar age of around 4.94 Gyr for L 98-59, indicating that the system’s planets could have experienced atmospheric escape for much longer than an age of  $>1$  Gyr predicts. In the meantime, while our results provide a broad view of the potential evolution of the L 98-59 planets, this broad view will be further constrained when combined with the next observations of the system.

Finally, in their analysis of a recent planet b transmission spectrum, Damiano et al. (2022) describe other potential models (besides cloud-free,  $\text{H}_2$ -dominated, and water-dominated) that include volatiles such as HCN,  $\text{CO}_2$ , CO,  $\text{N}_2$ , and  $\text{CH}_4$ , which our own simulations do not take into account. So while our results point to the possibility of a water-vapor and oxygen-dominated atmosphere on L 98-59 b, our predictions may be limited because our model assumes a high initial water content on the planet to achieve this result and does not account for a varied set of volatiles.

## 6. Conclusion

In this paper, we model the evolution of the L 98-59 system to study the effects of atmospheric escape on the potential volatiles present on the inner three planets. Consisting of three small, transiting, and likely rocky planets (and a fourth nontransiting planet) orbiting their M-dwarf star, this system is an ideal candidate to better characterize the atmospheric evolution of multiple terrestrial planets within the same stellar environment.

We run simulations with a parameter sweep of the system’s characteristics, giving the planets an initial water budget of either 1, 10, or 100 TO each and evolving them over several billion years. We gather the following results:

1. All three planets have experienced strong atmospheric escape due to their proximity to L 98-59 and the exposure to their star’s XUV and flare activity.
2. The smallest and closest planet, b, may counterintuitively retain water longer than c and d, because its exposure to a higher XUV flux leads to increased radiative cooling, and thus a lower escape efficiency.
3. Given enough starting water (100 TO) and depending on the system’s age, all three planets may still have water left over today, with the highest chances of detection being for planet b.
4. All three planets can accumulate significant quantities of oxygen created by water photolysis, from 15 bars up to thousands of bars.

Multiplanet systems can provide us with important insight on planet formation and evolution, orbital dynamics, and planetary architectures. Moreover, planets around bright, nearby stars such as L 98-59 are ideal targets for atmospheric characterization with emission and transmission spectroscopy

(Kostov et al. 2019). This system serves as an excellent case to study the development of multiple terrestrial planets and their atmospheres.

Further, the presence of an atmosphere on any of the L 98-59 planets is highly dependent on the way the planets evolved in the presence of their star's stellar activity and, specifically, the initial composition with which they began evolving. Therefore, our work studying the effects of flares and strong XUV radiation on volatile loss or accumulation for these planets may help us to better constrain certain characteristics of the system, such as stellar age, initial planetary composition, and planetary formation processes, in future observations with JWST.

### Acknowledgments

The material is based upon work supported by NASA under award No. 80GSFC21M0002. This research has made use of the NASA Exoplanet Archive, which is operated by the California Institute of Technology, under contract with the National Aeronautics and Space Administration under the Exoplanet Exploration Program. This research was carried out in part at the Jet Propulsion Laboratory, California Institute of Technology, under a contract with the National Aeronautics and Space Administration (grant No. 80NM0018D0004). R.B. acknowledges support from NASA grant No. 80NSSC23K0261. L.N.R.A. acknowledges the support of UNAM DGAPA PAPIIT project IN110420. L.N.R.A. thanks CONACYT's graduate scholarship program for its support. E.F.F. thanks Thaddeus D. Komacek for insightful discussions regarding simulation results, and Siddhant Solanki for their help with optimizing our code and running a set of our simulations during the revisions of this paper. We thank the anonymous referee for the insightful comments and valuable suggestions, which improved the overall quality of this paper.

*Software:* VPLanet (Barnes et al. 2020), mercury (Chambers & Murison 2000), jupyter (Kluyver et al. 2016), NumPy (Harris et al. 2020), SciPy (Virtanen et al. 2020), Matplotlib (Hunter 2007), Pandas (pandas development team 2020), SymPy (Meurer et al. 2017), seaborn (Waskom 2021), fitter (Cokelaer et al. 2023).

### ORCID iDs

Emeline F. Fromont  <https://orcid.org/0000-0002-3099-0493>

John P. Ahlers  <https://orcid.org/0000-0003-2086-7712>

Laura N. R. do Amaral  <https://orcid.org/0000-0002-8341-0376>


Rory Barnes  <https://orcid.org/0000-0001-6487-5445>

Emily A. Gilbert  <https://orcid.org/0000-0002-0388-8004>

Elisa V. Quintana  <https://orcid.org/0000-0003-1309-2904>

Sarah Peacock  <https://orcid.org/0000-0002-1046-025X>

Thomas Barclay  <https://orcid.org/0000-0001-7139-2724>

Allison Youngblood  <https://orcid.org/0000-0002-1176-3391>

### References

- Abe, Y. 1993, *Litho*, 30, 223  
 Baraffe, I., Homeier, D., Allard, F., & Chabrier, G. 2015, *A&A*, 577, A42  
 Barclay, T., & Gilbert, E. 2020, mrtommyb/xoflares, v0.2.1, Zenodo, doi:10.5281/zenodo.4156285  
 Barclay, T., Kostov, V. B., Colón, K. D., et al. 2021, *AJ*, 162, 300  
 Barclay, T., Sheppard, K. B., Latouf, N., et al. 2023, arXiv:2301.10866  
 Barnes, R., Luger, R., Deitrick, R., et al. 2020, *PASP*, 132, 024502  
 Barth, P., Carone, L., Barnes, R., et al. 2021, *AsBio*, 21, 1325  
 Billings, L. 2011, *Natur*, 470, 27  
 Bolmont, E., Selsis, F., Owen, J. E., et al. 2017, *MNRAS*, 464, 3728  
 Bonfils, X., Delfosse, X., Udry, S., et al. 2013, *A&A*, 549, A109  
 Bourrier, V., Lecavelier des Etangs, A., Ehrenreich, D., et al. 2018, *A&A*, 620, A147  
 Burke, C. J., Levine, A., Fausnaugh, M., et al. 2020, TESS-Point: High precision TESS pointing tool, Astrophysics Source Code Library, ascl:2003.001  
 Chambers, J. E., & Murison, M. A. 2000, *AJ*, 119, 425  
 Chassefière, E., Wieler, R., Marty, B., & Leblanc, F. 2012, *P&SS*, 63, 15  
 Chen, H., Zhan, Z., Youngblood, A., et al. 2021, *NatAs*, 5, 298  
 Chiang, E., & Laughlin, G. 2013, *MNRAS*, 431, 3444  
 Ciesla, F. J., Mulders, G. D., Pascucci, I., & Apai, D. 2015, *ApJ*, 804, 9  
 Cloutier, R., Astudillo-Defru, N., Bonfils, X., et al. 2019, *A&A*, 629, A111  
 Cloutier, R., & Menou, K. 2020, *AJ*, 159, 211  
 Cokelaer, T., Kravchenko, A., lahdjirayhan, et al. 2023, cokelaer/fitter: v1.5.2, Zenodo, doi:10.5281/zenodo.7497983  
 Damiano, M., Hu, R., Barclay, T., et al. 2022, *AJ*, 164, 225  
 Demangeon, O. D. S., Zapatero Osorio, M. R., Alibert, Y., et al. 2021, *A&A*, 653, A41  
 do Amaral, L. N. R., Barnes, R., Segura, A., & Luger, R. 2022, *ApJ*, 928, 12  
 Domagal-Goldman, S. D., Segura, A., Claire, M. W., Robinson, T. D., & Meadows, V. S. 2014, *ApJ*, 792, 90  
 Dressing, C. D., & Charbonneau, D. 2013, *ApJ*, 767, 95  
 Dressing, C. D., & Charbonneau, D. 2015, *ApJ*, 807, 45  
 Ehrenreich, D., Bourrier, V., Wheatley, P. J., et al. 2015, *Natur*, 522, 459  
 Engle, S. G., & Guinan, E. F. 2023, *ApJL*, 954, L50  
 France, K., Duvvuri, G., Egan, H., et al. 2020, *AJ*, 160, 237  
 Fujii, Y., Angerhausen, D., Deitrick, R., et al. 2018, *AsBio*, 18, 739  
 Gardner, J. P., Mather, J. C., Clampin, M., et al. 2006, *SSRv*, 123, 485  
 Gilbert, E. A., Barclay, T., Quintana, E. V., et al. 2022, *AJ*, 163, 147  
 Gillon, M., Triau, A. H. M. J., Demory, B.-O., et al. 2017, *Natur*, 542, 456  
 Greene, T. P., Line, M. R., Montero, C., et al. 2016, *ApJ*, 817, 17  
 Gronoff, G., Arras, P., Baraka, S., et al. 2020, *JGRA*, 125, e27639  
 Günther, M. N., Zhan, Z., Seager, S., et al. 2020, *AJ*, 159, 60  
 Hardegree-Ullman, K. K., Cushing, M. C., Muirhead, P. S., & Christiansen, J. L. 2019, *AJ*, 158, 75  
 Harris, C. R., Millman, K. J., van der Walt, S. J., et al. 2020, *Natur*, 585, 357  
 Hord, B. J., Kempton, E. M. R., Mikal-Evans, T., et al. 2023, arXiv:2308.09617  
 Howard, W. S. 2022, *MNRAS*, 512, L60  
 Hunter, J. D. 2007, *CSE*, 9, 90  
 Kane, S. R., Arney, G., Crisp, D., et al. 2019, *JGRE*, 124, 2015  
 Kane, S. R., Kopparapu, R. K., & Domagal-Goldman, S. D. 2014, *ApJL*, 794, L5  
 Kasting, J. F. 1988, *Icar*, 74, 472  
 Kasting, J. F., Whitmire, D. P., & Reynolds, R. T. 1993, *Icar*, 101, 108  
 Kempton, E. M. R., Bean, J. L., Louie, D. R., et al. 2018, *PASP*, 130, 114401  
 Kluyver, T., Ragan-Kelley, B., Pérez, F., et al. 2016, in Positioning and Power in Academic Publishing: Players, Agents and Agendas, ed. F. Loizides & B. Schmidt (Amsterdam: IOS Press), 87  
 Kopparapu, R. K., Ramirez, R., Kasting, J. F., et al. 2013, *ApJ*, 765, 131  
 Kopparapu, R. K., Ramirez, R. M., SchottelKotte, J., et al. 2014, *ApJL*, 787, L29  
 Koskinen, T. T., Lavvas, P., Huang, C., et al. 2022, *ApJ*, 929, 52  
 Kostov, V. B., Schlieder, J. E., Barclay, T., et al. 2019, *AJ*, 158, 32  
 Lammer, H., Kasting, J. F., Chassefière, E., et al. 2008, *SSRv*, 139, 399  
 Lammer, H., Zerkle, A. L., Gebauer, S., et al. 2018, *A&ARv*, 26, 2  
 Lecavelier des Etangs, A., Bourrier, V., Wheatley, P. J., et al. 2012, *A&A*, 543, L4  
 Lincowski, A. P., Meadows, V. S., Crisp, D., et al. 2018, *ApJ*, 867, 76  
 Louca, A. J., Miguel, Y., Tsai, S.-M., et al. 2023, *MNRAS*, 521, 3333  
 Luger, R., & Barnes, R. 2015, *AsBio*, 15, 119  
 Luger, R., Barnes, R., Lopez, E., et al. 2015, *AsBio*, 15, 57  
 Ment, K., & Charbonneau, D. 2023, *AJ*, 165, 265  
 Meurer, A., Smith, C. P., Paprocki, M., et al. 2017, *PeerJ Comput. Sci.*, 3, e103  
 Morbidelli, A., Chambers, J., Lunine, J. I., et al. 2000, *M&PS*, 35, 1309  
 Mordasini, C., Alibert, Y., Georgy, C., et al. 2012, *A&A*, 547, A112  
 Morley, C. V., Kreidberg, L., Rustamkulov, Z., Robinson, T., & Fortney, J. J. 2017, *ApJ*, 850, 121  
 Muirhead, P. S., Dressing, C. D., Mann, A. W., et al. 2018, *AJ*, 155, 180  
 Muirhead, P. S., Mann, A. W., Vanderburg, A., et al. 2015, *ApJ*, 801, 18  
 Murray-Clay, R. A., Chiang, E. I., & Murray, N. 2009, *ApJ*, 693, 23  
 Ogihara, M., & Ida, S. 2009, *ApJ*, 699, 824  
 Ostberg, C., Kane, S. R., Li, Z., et al. 2023, *AJ*, 165, 168

- Owen, J. E., Shaikhislamov, I. F., Lammer, H., Fossati, L., & Khodachenko, M. L. 2020, *SSRv*, **216**, 129
- Peacock, S., Barman, T., Shkolnik, E. L., et al. 2020, *ApJ*, **895**, 5
- Pidhorodetska, D., Moran, S. E., Schwieterman, E. W., et al. 2021, *AJ*, **162**, 169
- Pitkin, M., Williams, D., Fletcher, L., & Grant, S. D. T. 2014, *MNRAS*, **445**, 2268
- Pu, B., & Lai, D. 2019, *MNRAS*, **488**, 3568
- Quick, L. C., Roberge, A., Mlinar, A. B., & Hedman, M. M. 2020, *PASP*, **132**, 084402
- Quintana, E. V., Barclay, T., Raymond, S. N., et al. 2014, *Sci*, **344**, 277
- Ramirez, R. M., & Kaltenegger, L. 2014, *ApJL*, **797**, L25
- Raymond, S. N., Quinn, T., & Lunine, J. I. 2006, *Icar*, **183**, 265
- Raymond, S. N., Scalo, J., & Meadows, V. S. 2007, *ApJ*, **669**, 606
- Ribas, I., Guinan, E. F., Güdel, M., & Audard, M. 2005, *ApJ*, **622**, 680
- Ricker, G. R., Winn, J. N., Vanderspek, R., et al. 2015, *JATIS*, **1**, 014003
- Schindler, T. L., & Kasting, J. F. 2000, *Icar*, **145**, 262
- Shields, A. L., Ballard, S., & Johnson, J. A. 2016, *PhR*, **663**, 1
- Shkolnik, E. L., & Barman, T. S. 2014, *AJ*, **148**, 64
- Solomon, S. C. 1979, *PEPI*, **19**, 168
- Stelzer, B., Bogner, M., Magaúda, E., & Raetz, S. 2022, *A&A*, **665**, A30
- The pandas development team 2020, pandas-dev/pandas: Pandas, v2.2.0rc0, Zenodo, doi:10.5281/zenodo.3509134
- Tian, F., France, K., Linsky, J. L., Mauas, P. J. D., & Vieytes, M. C. 2014, *E&PSL*, **385**, 22
- Tian, F., & Ida, S. 2015, *NatGe*, **8**, 177
- Tian, F., Kasting, J. F., Liu, H.-L., & Roble, R. G. 2008, *JGRE*, **113**, E05008
- Tilley, M. A., Segura, A., Meadows, V., Hawley, S., & Davenport, J. 2019, *AsBio*, **19**, 64
- Unterborn, C. T., Desch, S. J., Hinkel, N. R., & Lorenzo, A. 2018, *NatAs*, **2**, 297
- Vidal-Madjar, A., Lecavelier des Etangs, A., Désert, J. M., et al. 2003, *Natur*, **422**, 143
- Villanueva, G. L., Smith, M. D., Protopapa, S., Faggi, S., & Mandell, A. M. 2018, *JQSRT*, **217**, 86
- Virtanen, P., Gommers, R., Oliphant, T. E., et al. 2020, *NatMe*, **17**, 261
- Waskom, M. L. 2021, *JOSS*, **6**, 3021
- Weiss, L. M., Marcy, G. W., Petigura, E. A., et al. 2018, *AJ*, **155**, 48
- West, A. A., Hawley, S. L., Bochanski, J. J., et al. 2008, *AJ*, **135**, 785
- West, A. A., Weisenburger, K. L., Irwin, J., et al. 2015, *ApJ*, **812**, 3
- Wetherill, G. W. 1990, *AREPS*, **18**, 205
- Wordsworth, R., & Pierrehumbert, R. 2014, *ApJL*, **785**, L20